Nanoscale

Accepted Manuscript

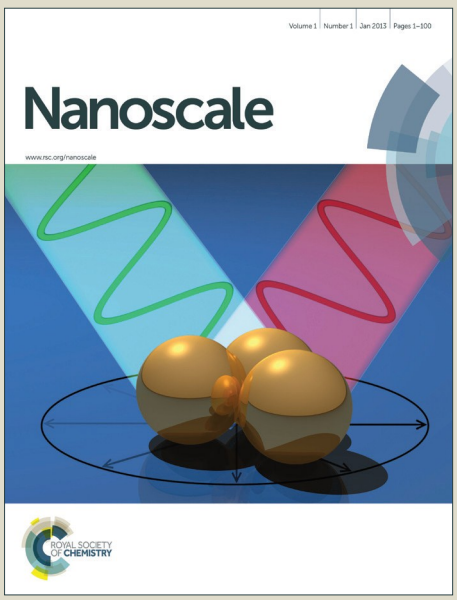

ROYAL SOCIETY OF CHEMISTRY

www.rsc.org/nanoscale

Nanoscale

COMMUNICATION

A sweet spot for highly efficient growth of vertically aligned single-walled carbon nanotube forests enabling their unique structures and properties

Received 00th January 20xx,
Accepted 00th January 20xx

DOI: 10.1039/x0xx00000x

www.rsc.org/

Guohai Chen,[*ab] Robert C. Davis,[c] Don N. Futaba,[*ab] Shunsuke Sakurai,[ab] Kazufumi Kobashi,[ab] Motoo Yumura[ab] and Kenji Hata[*ab]

We investigated the correlation between growth efficiency and structural parameters of single-walled carbon nanotube (SWCNT) forests and report the existence of a SWCNT "sweet spot" in the CNT diameter and spacing domain for highly efficient synthesis. Only within this region could SWCNTs be grown efficiently. Through the investigation of the growth rates for ~340 CNT forests spanning diameters from 1.3 to 8.0 nm and average spacing from 5 to 80 nm, this "sweet spot" was found to exist because highly efficient growth was constrained by several mechanistic boundaries that either hindered the formation or reduced the growth rate of SWCNT forests. Specifically, with increased diameter SWCNTs transitioned to multiwalled CNTs (*multiwall border*), small diameter SWCNTs could only be grown at low growth rates (*low efficiency border*), sparse SWCNTs lacked the requirements to vertically align (*lateral growth border*), and high density catalysts could not be prepared (*high catalyst density border*). As a result, the SWCNTs synthesized within this "sweet spot" possessed a unique set of characteristics vital for the development applications, such as large diameter, long, aligned, defective, and high specific surface area.

Although classified with a single term, "carbon nanotube" (CNT), this carbon allotrope can vary significantly in terms of its structure and characteristics. Apt examples are chirality, diameter, length, crystallinity, purity, and wall number. Taming the growth of CNTs is central to control the structure and characteristics of the CNTs, and despite the significant effort devoted over the past two decades, it remains a challenging topic highlighted by the recent report of selective chirality growth.[1]

A unique example of the structural control of CNTs is to grow them from an array of closely packed catalysts and uti… the crowding effect to enable them to vertically self-align into… bulk material, called a "forest". The CNTs within the forest have itself proven to possess a unique set of structural properties not possible by other synthesis methods, *e.g.* long, aligned, pur… and possessing high specific surface area (SSA). Therefore, the… CNT forest has opened up many new and important application…, spanning a wide range of fields, such as field emitters,[2] touch… panels,[3] planar incandescent light sources,[4] flexible cha… collectors,[5] high power and density supercapacitors,[6,7] gecko… foot-mimetic dry adhesive,[8] bristles/brush,[9,10] through silico… vias,[11] and high current-carrying capacity CNT-Cu composites.[12]

Encouraged by the development of new applications whic… is unique to CNT forests, a significant effort has been carried ou… to improve their synthesis through chemical vapor depositio… (CVD).[8,13-30] In particular, a substantial effort has been carried out to tune the structures, such as diameter, length, density, alignment *etc*. to meet the specific demands of applications. For example, Esconjauregui *et al* controlled the catalyst density to tune the single-walled CNT (SWCNT) areal density from 10^{12} to 10^{14} cm^{-2} that is important for via interconnect applications.[30] Qu *et al* developed a method to synthesize a forest with a curl… entangled top surface and realized a dry adhesive tape with 10… times stronger adhesive force than a gecko foot.[8] By introducing Mo into the catalyst, Xiang *et al* succeeded in controlling the… SWCNT diameter from 2.5 to 1.2 nm and demonstrated it use… for optical and electronics applications.[14] Similarly, catalyst… fabrication by arc plasma deposition and controlling the catalyst… formation process have demonstrated wide range control o… the diameter.[27,31] By controlling the active catalyst density, Xu… *et al* controlled both the spacing between the CNTs (from 6 t… 65 nm) and the alignment in the forest from 0.13 (nearly… random) to 0.85 (nearly perfectly aligned) as evaluated by the… Herman's Orientation Factor (HOF) and showed that the non… aligned forest possessed rubber-like temperature invariant… viscoelasticity.[23,32] These examples demonstrate the potential… to synthesize forests of diverse structure which, in turn, provide… very different physical and chemical properties. Moreover, the…

[a] *Technology Research Association for Single Wall Carbon Nanotubes (TASC), Central 5, 1-1-1 Higashi, Tsukuba, Ibaraki, 305-8565, Japan. Currently at Brigham Young University, Provo, Utah 84602, USA. E-mail: guohaichen@gmail.com*
[b] *National Institute of Advanced Industrial Science and Technology (AIST), Central 5, 1-1-1- Higashi, Tsukuba, Ibaraki, 305-8565, Japan. E-mail: kenji-hata@aist.go.jp, d-futaba@aist.go.jp*
[c] *Department of Physics and Astronomy, Brigham Young University, Provo, Utah 84602, USA.*

Electronic Supplementary Information (ESI) available: Detailed experimental processes for each catalyst preparation method and CNT synthesis process. See DOI: 10.1039/x0xx00000x

suggest that the key parameters for structural control are catalyst size and spacing.

These researches show that SWCNT forests are advantageous for many applications; however, to develop them into real commercial products, the industrial scale mass production of SWCNT forests is of paramount importance. There has been significant effort to develop synthetic approaches for mass production of CNT forests. For example, de Villoria *et al* has developed a continuous CVD furnace with a conveyance to grow multiwalled CNT (MWCNT) forests.[22] Wei *et al* has demonstrated a pilot plant fluidized-bed reactor to grow agglomerated and vertically aligned CNTs.[33] Furthermore, a commercial ton-scale factory is currently under construction for the continuous synthesis of SWCNT forests where substrates are fed into a furnace by belt conveyer.[34] In such system, the growth yield (CNT weight per substrate area), Y, could be estimated as Y = W×L×D×R, where W and L are the width and length of the furnace, D is the density of the forest, and R is the growth rate. The growth temperature is about 800 °C, which imposes a physical limitation to the length and width of the furnace. The density of the forest can be increased to some level; however, as the catalyst is distributed across the substrate, the gas diffusion becomes difficult, which reduces forests height, and thus limits the production rate. From these limitations, a fast growth rate (highly efficient growth) becomes indispensable to realize mass production. However, at this stage, it is not understood if the synthesis of various forests with different structures as described above is possible while maintaining highly efficient growth. This is because the correlation between the growth rate (growth yield) and structural parameters, such as diameter, density, alignment, crystallinity, *etc*. is unknown.

In this work, we address this important issue by studying the growth rate (growth yield) for ~340 CNT forests synthesized across a wide range of structural parameters. Through this work, we discovered a region within the phase space of CNT diameter and catalyst spacing, *i.e*. "sweet spot", within which the highly efficient growth of SWCNT forests was confined. We revealed that the highly efficient SWCNT forest sweet spot exists because it is constrained by several mechanistic boundaries that either hinders the formation or reduces the growth rate of SWCNT forests. Specifically, large SWCNTs transitioned to MWCNTs (*multiwall border*) while small SWCNTs could only be grown with low growth rates (*low efficiency border*). Moreover, sparse SWCNTs lost their ability to vertically align (*lateral growth border*) and for dense SWCNTs, we were unable to achieve such high catalyst density without experiencing aggregation (*high catalyst density border*). As a result of this restriction in the CNT diameter and spacing, the synthesized SWCNTs possessed a unique set of characteristics, such as large, long, aligned, defective, and high SSA. These characteristics were crucial to develop applications and were the key to the commercialization of SWCNT forests.

The synthesis of an extensive family of CNT forests encompassing a wide range of structural parameters was central to this work as displayed in Figures 1 and 2. Our approach to prepare this family was based on water-assisted CVD carried out on various Fe catalyst systems that have different catalyst size (1.3 to 8.0 nm) and spacing (5 to 80 nm). Water-assisted CVD is known to represent one of the high growth efficiency methods with very fast growth rate and high growth yields and is also suited to grow SWCNT forests.[13] In addition, a commercial factory under construction employs this method.[34] Therefore, we think that this method is appropriate to study the correlation between growth efficiency and structural parameters of the SWCNT forest. For our growth conditions, we chose a general procedure adaptable to most catalyst conditions and could provide the highest growth yield. Specifically, either ethylene or acetylene was used as a carbon source, and water was used as a growth enhancer at a typical growth temperature of ~750 °C. The detailed recipe is described in the super-growth CVD manual and available online.[35] We wish to note that optimization of the synthesis process was limited to carbon concentration, water content, and growth temperature. We accumulated data from ~340 different CNT forests synthesized by various Fe catalysts. The methods employed to deposit the catalysts were: arc plasma Fe/Fe-alloy nanoparticle deposition, sputtered Fe thin films of different thicknesses, sputtered aluminium-capped Fe catalysts, and $FeCl_3$ nanoparticles deposited by wet chemistry. In addition, we treated these catalysts by reactive ion etching (RIE), oxidation at different temperatures and ambients, and finally reduced the catalyst systems at different temperatures, times, and flow rates.[26,27,31,32,36-38]. In this way, we succeeded in modulating the catalyst size and spacing spanning across an unprecedented wide range from 1.3 to 8.0 nm and 5 to 80 nm, respectively, and as a result encompassing all the major reported varieties of CNT forests, including tall and short vertically-aligned SWCNT forests, 2~3 walled CNT forests, MWCNT forests, non-aligned CNT forests, and lateral SWCNT agglomerates as displayed schematically in Figures 1c-1h.

The heights of each member of this large family of ~340 CNT forests were plotted as a function of the catalyst size and catalyst spacing to generate two-dimensional maps (Figures 1 and 2). One map shows the full-range spanning from SWCNT to MWCNT forests (Figure 1a) while the second map focuses on the SWCNT zone (Figure 2). In the full-range map (Figure 1a) the different CNT wall numbers, as determined by >4 transmission electron microscopy (TEM) observations for each of the catalyst conditions, were represented by colours, *i.e.* red: SWCNTs, blue: double- or triple-walled CNTs (2~3WCNTs), and green: MWCNTs. Six CNT forests and their catalysts representing the MW-, 2~3W-, and SWCNT zones (non-aligned CNT forests, lateral SWCNT agglomerates, tall and short vertically-aligned SWCNT forests) are displayed by the scanning electron microscopy (SEM) and atomic force microscopy (AFM) images, respectively (Figures 1c-1h). The CNTs grown in these six zones were also analysed by TEM to estimate their diameter ranges. The size distributions for the CNTs and catalysts showed good agreement with the exception of the MWCNT zone (Figure 1c). In the SWCNT zone map, the colours represent the different growth efficiencies as defined by the height of the vertically aligned forests synthesized in a 10 minute growth time (*e.g*

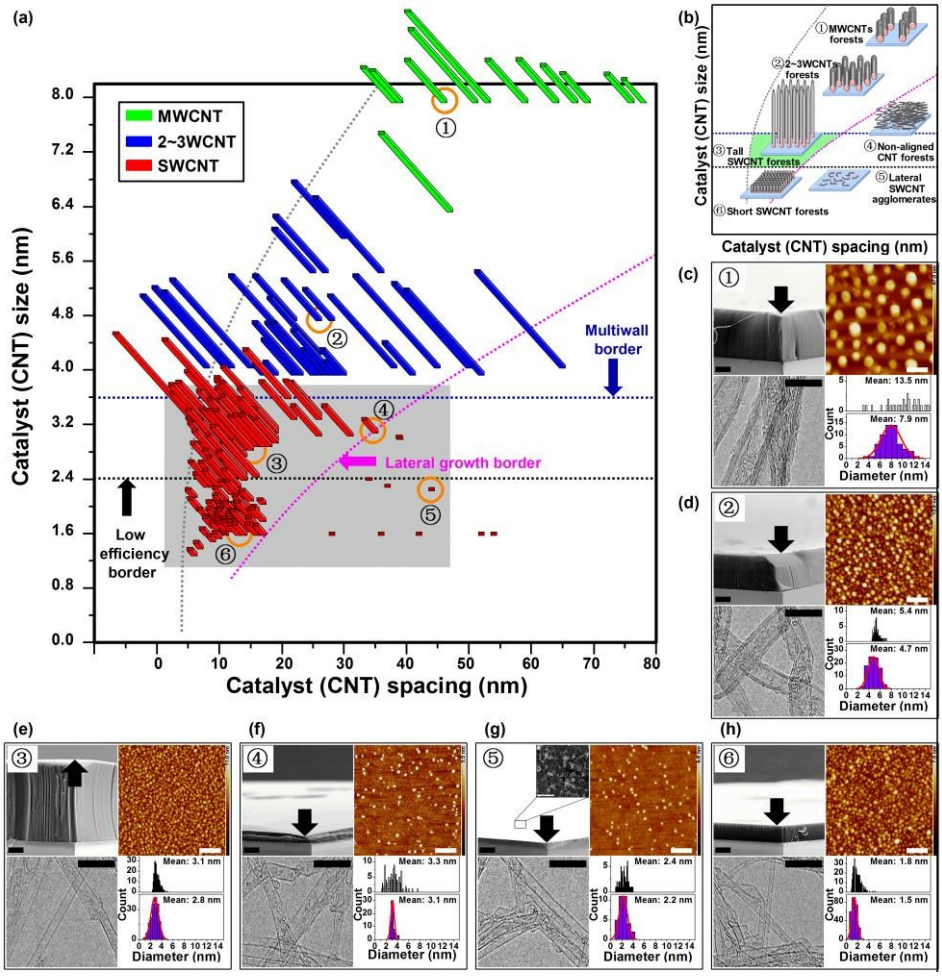

Figure 1. (a) Full-range map showing the multiple borders for forest height as a function of catalyst (CNT) size and spacing. The colours represent the wall number selectivity and the gray rectangle indicates the SWCNT zone. (b) Schematic of the individual regions and (c)-(h) Characterization of representative CNTs in each of the regions of (a): SEM, AFM, TEM images, catalyst size distributions (upper) and CNT diameter histograms (lower). Scale bars: 200 μm for SEM; 100 nm for AFM; 10 nm for TEM.

yellow: <100 μm, orange: 200-300 μm, and pink: >400 μm) (Figure 2).

There are several important points highlighted by these maps. First, all the results from the different catalyst methods merged together to form a smooth and continuous landscape without exhibiting significant discontinuities at the boundaries between preparation methods. This is direct evidence that the catalyst diameter and spacing are two critical parameters that determine the structure of the CNT forest, and the method by which they are prepared is irrelevant. For the alumina/Fe catalyst, it has been proposed that the Ostwald ripening and subsurface diffusion are balanced to create an equilibrium catalyst particle size.[38] We interpret that, in such case, the difference in the preparation method might not be a vital factor in determining the diameter and spacing of catalysts.

Second, as evidenced in the SWCNT zone map, highly efficient growth of SWCNT forests occurred exclusively within a distinct region of catalyst size and spacing (Figure 2). Herein represents the main finding of this report. Every catalyst system (size and spacing) within this region demonstrated the ability to growth efficiently. For this work, we defined "highly efficient growth" as the condition when the forest height exceeded ~400 μm in a 10 min growth time. Guide lines are added to the figures to guide the eyes based on experimental data. Therefore, wit[h] this work, efficiency is respect to time. The 400 μm in 10 minute growth time was chosen from a practical aspect such that it represents a sustained growth rate/catalyst activity of at leas[t] 40 μm/min. In addition, without exception, every catalys[t] condition outside this region did not demonstrate the abilit[y] grow efficiently even after optimization. Therefore, by thes[e] criteria, we define this region as the "sweet spot" for highl[y] efficient SWCNT forest synthesis. The sweet spot was centere[d] at the catalyst size of ~3 nm and catalyst spacing of ~17 nm an[d] this is exactly the condition where we first reported super growth SWCNT forest to grow millimeter-scale forests in 1[0] min.[13,39] The sweet spot was confined to a narrow regio[n] encompassing a range of catalyst size from ~2.4-~3.6 nm an[d] catalyst spacing from ~8-~35 nm.

Third, we found that this confinement of the sweet spot wa[s] due to multiple boundaries reflecting different mechanisms that either hindered the formation or reduced the growth rat[e] of SWCNT forests. Above a ~3.6 nm catalyst size (*multiwall border*), we observed the formation of DWCNTs and MWCNTs and below ~2.4 nm catalyst size threshold, small SWCNTs co[uld]

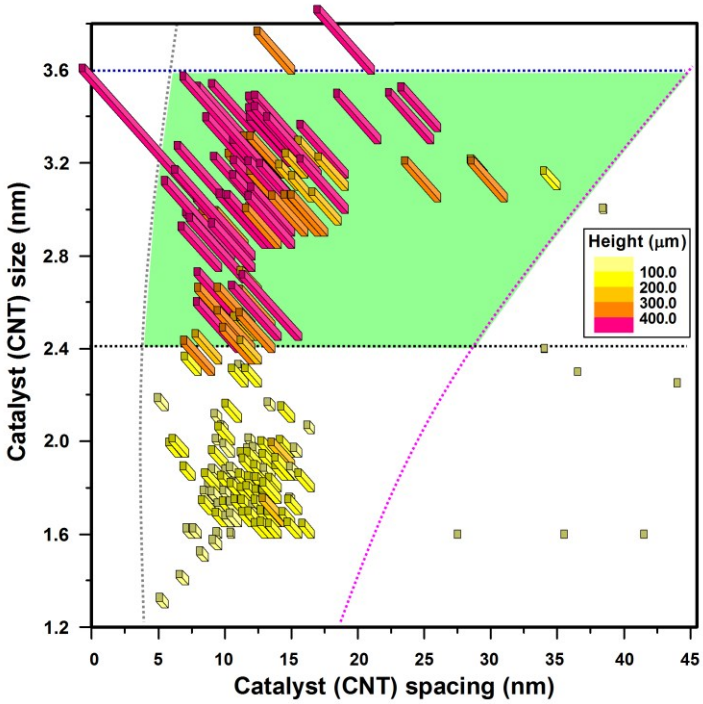

Figure 2. A map of the SWCNT growth region highlighting the region of high efficient growth, "sweet spot" (green area). Colours indicate levels of growth efficiency.

only be grown at low growth rates (*low efficiency border*). Furthermore, above ~35 nm catalyst spacing, the sparse SWCNTs lost their ability to vertically align (*lateral growth border*), and we could not achieve catalyst spacing below ~5 nm due to catalyst aggregation (*high catalyst density border*).

To understand what made the sweet spot so special, we performed an extensive investigation of the three borders surrounding the sweet spot. To this end, we prepared cross-sectional plots, as displayed as arrowed lines (indicated by colours and numbers) in the full range map, traversing the sweet spot, across the borders, and through the neighboring zones (Figure 3a). First, the *low efficiency border* was examined by a plot of the forest height as a function of diameter in the spacing range of 12-15 nm (Figure 3b). We found that the forest height dramatically decreased beyond the threshold catalyst size of ~2.4 nm. In addition, we created a similar plot using data taken from ~14 published reports,[13-17,25,27,28,40-45] and interestingly found a very similar trend showing that millimeter-scale SWCNT forests were solely grown with at a SWCNT diameter of ~3 nm and never from smaller diameter catalysts (Figure 3c). The similarity between our results and the literature shows the generality of phenomenon causing the border emphasizing the difficulty in achieving highly efficient growth with small diameter regardless of the CVD techniques. To clarify, the height of the forest results from a combination of the individual CNT growth rate and the forest alignment. Therefore, either a decrease in the growth rate of an individual SWCNT or a decrease in the ability for the assembly to grow vertically would result in a reduction in the forest height. We believe that both factors contribute to explain the existence of this border. Recent reports have shown that the rate at which carbon atoms can be converted to CNTs was fixed for each atom in the catalyst particle, and in such case the growth rate of SWCNT forest would be roughly proportional to the square of CNT diameter.[28,31] Therefore, a decrease in diameter would lead to a proportionate decrease in growth rate. In addition, the required forest density, *i.e.* inverse of inter-tube spacing, increases nonlinearly with decrease in the diameter.[31] Thus, as the diameter decreases for a fixed catalyst spacing, the growth rate of the forest decreases resulting in a shorter forest because of the decreased growth rate of the individual SWCNTs and the decreased ability of the aggregate to growth vertically. Hence, the growth efficiency reduces. Along the *low efficiency border*, as the catalyst spacing decreases and the catalyst size is fixed, a slight increase in forest height is observed, which is consistent with the increased ability to grow vertically. Unfortunately, the contributions of other mechanisms become significant, such as catalyst ripening and gas diffusion, which results in either the increase of SWCNT diameters (close to ~3 nm), or the decrease of the forest growth rate.

Second, the *lateral growth border* was examined by two plots: the level of alignment (as defined as HOF) and forest height as a function of spacing for CNT diameter of 3 (SWCNT) and 4 (DWCNT) nm. At small spacings (<~15 nm), both SWCNT and DWCNT forests possessed similar levels of alignment (~0.6-~0.8), but as the catalyst spacing increased, the SWCNT forests decreased in alignment more quickly than DWCNT forests (Figure 3d). For example, SWCNT forests lost alignment (defined by HOF <~0.2) at a catalyst (CNT) spacing of ~38 nm, while DWCNT forests lost alignment at ~65 nm. The difference between SWCNTs and DWCNTs became more evident in the plot of the forest height (Figure 3e). The SWCNT forest height

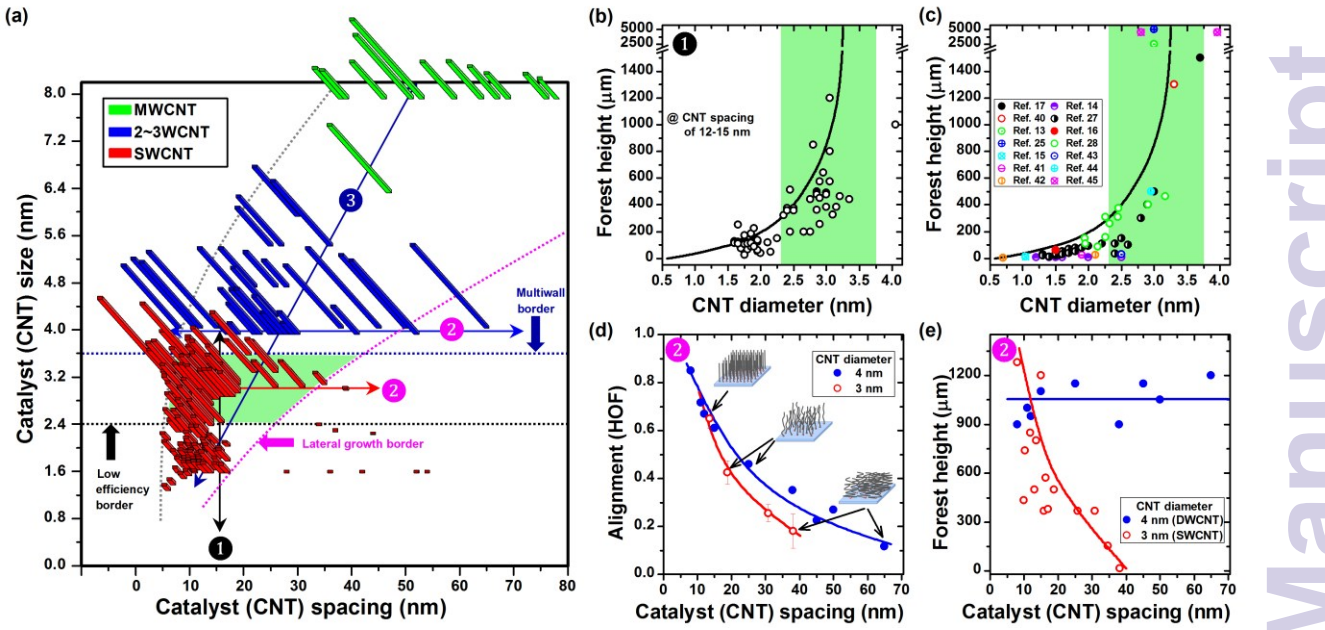

Figure 3. (a) The locations for cross-sectional plots of every structure (forest height, alignment, Raman G/D ratio, and SSA) as indicated by arrowed lines with colours and circled numbers. (b) Forest height as a function of CNT diameter at CNT spacing of 12-15 nm. (c) Literature survey shows tall forests are solely grown with a SWCNT diameter of [illegible] nm. (d) Alignment level (HOF) and (e) forest height as a function of catalyst (CNT) spacing for CNT diameter of 3 and 4 nm. Inset: schematics for different levels of alignment.

dropped dramatically with increased catalyst (CNT) spacing and at ~38 nm transitioned into lateral growth. As a result the range within which the SWCNT forests can be grown was very limited (~8-~35 nm). In contrast, for DWCNTs, the forest height remained high (~1000 μm) and relatively constant meaning that the range within which the DWCNT forests can be grown efficiently was much wider. It has been proposed that the "crowding effect" of CNTs is the mechanism of vertical alignment and that the flexural modulus (stiffness) of the CNT is an important physical parameter that governs the level of spacing that CNTs can self-assemble to align vertically.[32] The trends observed in our experimental match very well with this model because DWCNTs possess a higher flexural modulus than SWCNTs.

As demonstrated, the highly efficient growth region, "sweet spot" is limited to a zone only possessing the appropriate combination of CNT diameter and catalyst spacing. The requirements for highly efficient growth impart a unique set of structures and properties on the grown SWCNTs. In the sweet spot, a catalyst of ~3 nm is spaced by ~15 nm and withstands the growth temperature for ~10 min. This requires the catalyst to be bound to the surface very strongly as otherwise they will diffuse and aggregate. This has been evidenced by an x-ray photoelectron spectroscopy report that showed a strong interaction between the Fe catalyst and the Al_2O_3 support.[46] As a result of this strong binding, when the SWCNT forest is removed from the substrate, most of the catalyst remains on the substrate and the resultant as-grown material possesses an extremely high carbon purity (up to 99.98%).[13]

However, highly efficient growth does have a drawback since it is not possible to grow large diameter SWCNTs (~3 nm) at high speed without introducing many defects. This point is illustrated by a plot showing the level of crystallinity, as represented by the ratio of Raman Graphitic-band to Disorder-band intensity (G/D ratio) calculated from the Raman spectra and the height (growth rate) versus the CNT diameter (Figure 4a, 4b). The plot starts from the low efficiency zone with small diameter (~2 nm), continues through the sweet spot with large diameter (~3 nm), and extends through the multiwall zone (~8 nm), as illustrated in Figure 3a. The crystallinity and height (growth rate) showed an opposite trend, *e.g.*, when diameter was small (~2 nm), the G/D ratio was estimated to be as high as ~70, although it decreased to ~10 within the sweet spot. Computer simulations have shown that when carbon precipitates from the catalyst they form a very defective structure which "heals" into a CNT.[47] The crystallinity of the CNTs is determined by the balance between the precipitation process and the healing process. The speed of the precipitation process is the growth rate. Therefore, fast growth will inevitably lead to a defective CNT.

The combination of being large and defective is advantageous in terms of accessible surface area. This point is demonstrated by a plot of the Brunauer-Emmett-Teller SSA versus CNT diameter as calculated from the liquid nitrogen adsorption-desorption isotherms (Figure 4c) spanning from the low efficiency zone (~2 nm), through the sweet spot (~3 nm) and into the multiwall zone (~8 nm), as illustrated in Figure 3a. The SSA exceeded 1000 m^2/g for the SWCNTs (~2 and 3 nm) which is much larger than 600 m^2/g of small diameter (~1 nm) SWCNTs (*i.e.* purified HiPco) and approaches the theoretical value for the SSA for one side of a graphene sheet (Figure 4d).[3] As the wall number increased, the SSA rapidly decreased as expected.[36,48,49] As shown in the schematic (Figure 4e) and evidenced in the TEM images, the defective and large SWCNTs

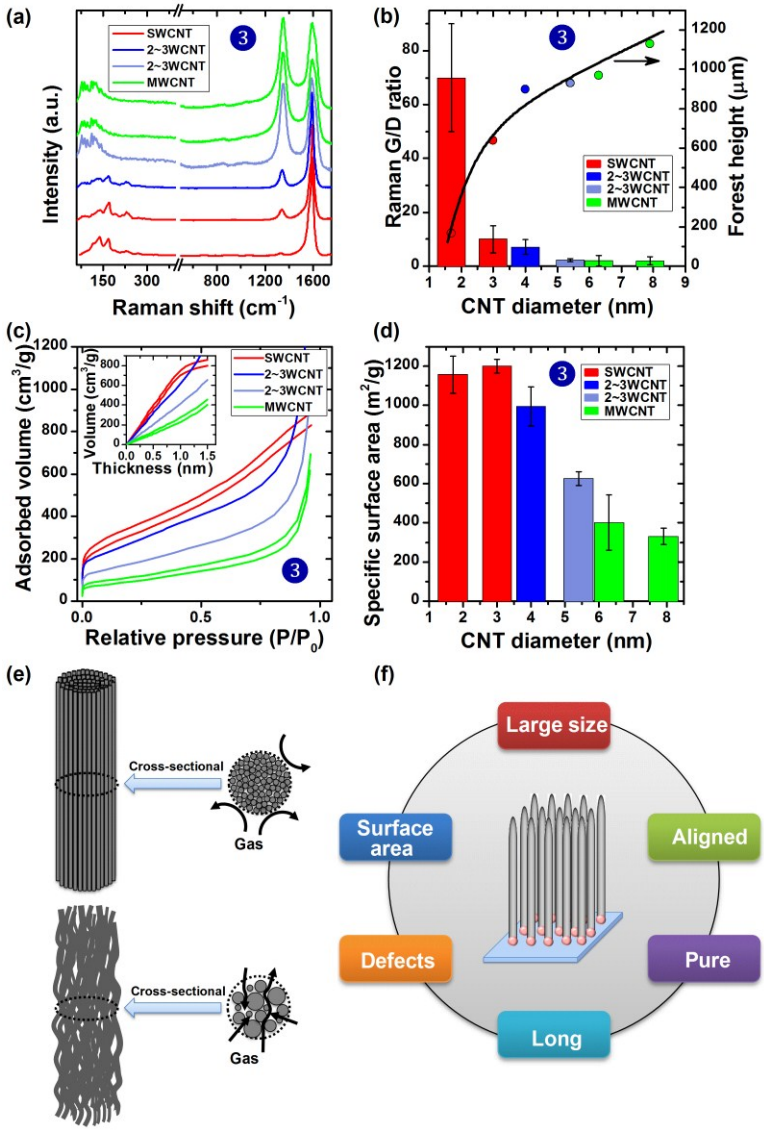

Figure 4. (a) Raman spectra, (b) Raman G/D ratio and forest height as a function of CNT diameter, (c) Adsorption isotherms for N_2 at 77 K (Inset: t-plot), and (d) SSA as a functi of CNT diameter, for SW-, 2~3W-, and MWCNT forests. (e) Schematics demonstrating the difference in pore structure between large/defective and small/straight SWCNTs. (f) Unique set of characteristics of SWCNT forests highly efficiently grown from the sweet spot.

(~2-3 nm) are wavy and possess many pores between them to allow nitrogen access to these interstitial areas of the CNT bundles while, in contrast, a bundle of small diameter (~1 nm) SWCNTs does not have sufficient spacing between CNTs for the nitrogen to diffuse within the bundle.

Stemming from fundamental mechanisms, highly efficient growth from the sweet spot results in SWCNTs that possess a unique set of characteristics as being large size, very long, highly pure, defective, aligned, and possessing very high SSA (Figure 4f). As evidenced in the specification table, the SWCNTs grown from the sweet spot show the highest purity, highest SSA, longest length among commercial SWCNTs and MWCNTs (Table 1). These outstanding characteristics were found to be essential to develop applications showing a significant improvement in performance when compared with other CNTs. These specific applications were the key to the commercialization of SWCNTs grown from the sweet spot. It is worth noting that applications of CNTs would inevitably introduce a number of additiona factors which contribute to the application performance, s as processing, dispersion, filtration, composite material mixing etc. However, the property aspects of the CNT growth ar important for nearly every application, such as the length, th accessible SSA, the purity. For example, the long length high SS which results from the high single wall selectivity and hig purity, were advantageous to fabricate highly conductive an mechanically robust CNT-rubber composites because th SWCNTs could easily deform in concert with the rubber matr with minimum stress concentration.[50] The high purity showed to be of great benefit to introduce the SWCNTs into the stric clean room environments necessary for semiconductor processing and to develop devices, such as CNT non-volati memory.[51] The combination of the SSA and purity was crucial to develop a CNT supercapacitor.[7,52-54] The high surface area was

Table 1. Specification sheet of commercialized CNTs.

CNT	Make	Grade	Carbon purity (%)	Diameter (nm)	Length (μm)	Bulk density (g/cm^3)	SSA (m^2/g)	G/D ratio	Combustion temperature (°C)
MWCNT	Showa Denko (Japan)	VGCF	>90	50-150	10-20	0.04	13		
		VGCF-X		10-15	3	0.08			
	CNT Co., LTD (Korea)	C100	>95	20	1-25	0.03-0.05	150-250		544
	Nanocyl (Belgium)	NC7000	90	9.5	1.5	0.043	250-300		
	Bayer MaterialScience (Germany)	Baytube C150P	>95	13-16	1->10				
	Ad-Nano Technologies (India)	ADCNT	>95	12	~20		50-220		
	CNano Technology (USA)	FloTube 9000	>95	11	10	0.03-0.15	>=200		
	Hodogaya Chemical (Japan)	XNRI	>99.5	40- 90		0.005-0.01	125-300		736
	XinNano Materials (Taiwan)	XNM-HP-15000	82%	8	>10		323	3.2	
	AVANSA Technology & Services (India)	MWCNTs	>97	10-20	10-30	0.22	>200		
SWCNT	**AIST (Japan)**	**SG-CNT**	**99.9**	**3**	**>300**	0.037	**>800**	7-10	618
	AIST (Japan)	e-DIPS	>95	0.7-2		0.03-0.04	400-1000	>100	
	Unidym (USA)	HiPco pure	>85	0.8-1.2	0.1-1.0		~400-1000		~470-490
	SouthWest Nanotechnoliges (USA)	CG200 (CoMoCAT)	90	1.3	0.4-2.3	0.091		>10	465
		CG300	95	0.84		0.128	770	>20	515
		SG65i	95	0.78	1.5	0.094	790		519
	Meijo Nano Carbon (Japan)	SWNT SO	>90	1.4	1-5			>100	
	Thomas Swan (UK)	Elicarb SWNT	>90	2	1		>700	>22	
	Sun Innovation (USA)	SWNT powder	95	1-2	5-30	0.03	405		
	XP Nano Material (China)	HS-WCNTS-90	>90	<2	5-30	0.14	380	>20	610
	Chengdu Alpha Nano Technology (China)	GYS001	>80	1-2	5-20		>400		
	OCSiAl (Russia)	TUBALL	>85	1.8	>5		~500	~75	750

All the data were collected from the homepage of each provider.

important for high energy density, and the purity was vital to achieve high operational voltage of 4 V and long cycle lifetime.[52]

The ability to control the catalyst size and spacing over a wide range was critical to enable to carry out this systematic investigation and reveal this sweet spot. As no single catalyst preparation method could cover this entire range, we used nearly every reported method to tune the Fe/Fe-alloy catalyst size and spacing. In general, the approaches to tune the catalyst size and spacing can be categorized into two general methods: 1) What and how the catalyst is deposited and 2) how the catalyst is treated prior to growth. The methods we employed to deposit the catalysts were: arc plasma Fe/Fe-alloy nanoparticle deposition, sputtered Fe thin films of different thicknesses, sputtered aluminium-capped Fe catalysts, and $FeCl_3$ nanoparticles deposited by wet chemistry.[26,27,36-38] Treatment of the catalyst prior to synthesis included exposure to RIE, oxidation at different temperatures and ambients, and finally reduction at different temperatures, times, and flow rates.[31,32]

In order to visualize the control range of each method, we constructed a "World map of catalyst preparation methods", by plotting the control ranges of every preparation method in terms of catalyst size versus spacing in different colours (Figure 5). From this world map several important points can be seen. First, the method which spanned the widest range was controlling the thickness of the catalyst film, that is, the amount of catalyst.[36,37] However, the limitation of this method was the strong correlation between the catalyst size and spacing because upon conversion from film to nanoparticles, large particles were separated with large spacing and small particles were separated by small spacing, making it impossible to independently tune the size and spacing.[36,37] As a result, the majority of the points fell along a line where the catalyst spacing increased with diameter, and we found it difficult to access the large catalyst spacing zone and the small catalyst size zone. Therefore, to access the small catalyst size zone, we employed different deposition methods, such as arc plasma deposition,[27] that could directly deposit small catalysts on the substrate, and aluminium capping,[26] that limited the diffusion of Fe thus providing smaller catalysts. Moreover, in order to access the larger catalyst spacing zone, we used special growth pretreatments, such as RIE exposure and extension of the pre-growth annealing time to reduce the number of active catalysts by either removal or deactivation.[31,32] To achieve very small catalysts with large spacing we used wet chemistry to directly synthesize small particles on the substrate.[38] The detailed experimental processes for each catalyst preparation method and CNT synthesis process can be found in Electronic Supplementary Information (ESI). Here, each of the catalysts were deposited onto an alumina support layer, since it has been difficult to grow forests on different supports.[46,55] It would be

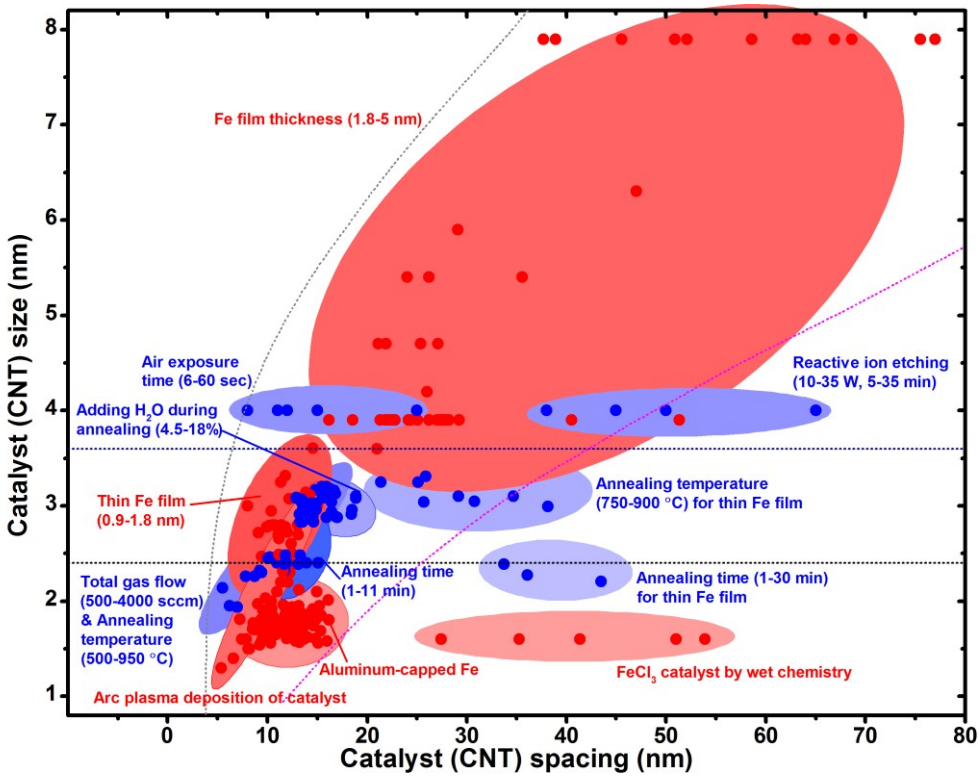

Figure 5. World map of catalyst preparation methods.

interesting to see different maps made from different support layers.

Finally, we do recognize that the synthesis of CNTs encompasses numerous factors including, but not limited to machine design, carbon sources, carrier gas species, catalyst, and catalyst preparation method, *etc.*, and in this work, optimization of the synthetic conditions was limited to carbon level, water level, and temperature. While we do expect that further optimization of the synthesis including those factors listed above could result in variations to our data, the existence of a sweet spot will not change significantly due to fundamental limitations on the catalyst and nanotubes to form a forest structure. We hope our work invokes future research in these directions.

Conclusions

We investigated the correlation between growth efficiency and structural parameters of SWCNT forests by examining the growth efficiency for ~340 CNT forests. This large set of CNT forests spanned an unprecedented wide diameter (1.3 to 8.0 nm) and catalyst spacing (5 to 80 nm) range, and as a result encompassed all the major reported varieties of CNT forests, including tall and short vertically-aligned SWCNT forests, 2~3 walled CNT forests, MWCNT forests, non-aligned CNT forests, and lateral SWCNT agglomerates. From this investigation, we revealed the existence of a SWCNT "sweet spot" in the catalyst (CNT) diameter and spacing domain for highly efficient synthesis. This "sweet spot" was confined by four mechanistic boundaries that either hindered the formation or reduced the growth rate of SWCNT forests: 1) the transition to MWCNTs (*multiwall border*); 2) the drop in growth efficiency (*low efficiency border*); 3) inability to vertically align (*lateral growth border*); and 4) high density catalyst zone (*high catalyst density border*). As a result, only within this "sweet spot" was the highly efficient growth of SWCNT forests possible and the resultant SWCNTs possessed a unique set of characteristics vital for the development applications, such as large diameter, long, aligned, defective, and high SSA.

Experimental

CNT synthesis. CNTs were synthesized by the water-assisted CVD method at ~750 °C using 1-7.5% C_2H_4 as the carbon feedstock (3-5% C_2H_2 for MWCNTs), water as the growth enhancer, and with He as the carrier gas.

Characterization. The catalyst nanoparticles were characterized by AFM (BRUKER Dimension FastScan). The CNTs were observed by SEM (Hitachi S-4800). The average diameter of SWCNTs were evaluated by Fourier transform infrared (FTIR, Nicolet 6700) spectroscopy by converting the position of S_{11} absorbance peak and confirmed by diameter histograms obtained from TEM (Hitachi H-9000NA) observation. For CNT forests, the CNT spacing was calculated from the CNT diameter and the forest mass density.[39] For lateral SWCNT agglomerates, the spacing was calculated from AFM images, assuming that the CNT diameter and spacing are identical to the catalyst size and spacing, respectively.

Acknowledgements

This paper is based on results obtained from a project Commissioned by the New Energy and Industrial Technology Development Organization (NEDO).

Notes and references

1 F. Yang, X. Wang, D. Q. Zhang, J. Yang, D. Luo, Z. W. Xu, J. K. Wei, J. Q. Wang, Z. Xu, F. Peng, X. M. Li, R. M. Li, Y. L. Li, M. H. Li, X. D. Bai, F. Ding and Y. Li, *Nature*, 2014, **510**, 522.
2 G. H. Chen, D. H. Shin, T. Iwasaki, H. Kawarada and C. J. Lee, *Nanotechnology*, 2008, **19**, 415703.
3 C. Feng, K. Liu, J. S. Wu, L. Liu, J. S. Cheng, Y. Y. Zhang, Y. H. Sun, Q. Q. Li, S. S. Fan and K. L. Jiang, *Adv. Funct. Mater.*, 2010, **20**, 885.
4 M. Zhang, S. L. Fang, A. A. Zakhidov, S. B. Lee, A. E. Aliev, C. D. Williams, K. R. Atkinson and R. H. Baughman, *Science*, 2005, **309**, 1215.
5 J. T. Di, D. M. Hu, H. Y. Chen, Z. Z. Yong, M. H. Chen, Z. H. Feng, Y. T. Zhu and Q. W. Li, *ACS Nano*, 2012, **6**, 5457.
6 W. Lu, L. T. Qu, K. Henry and L. M. Dai, *J. Power Sources*, 2009, **189**, 1270.
7 Y. Q. Jiang, P. B. Wang, X. N. Zang, Y. Yang, A. Kozinda and L. W. Lin, *Nano Lett.*, 2013, **13**, 3524.
8 L. T. Qu, L. M. Dai, M. Stone, Z. H. Xia and Z. L. Wang, *Science*, 2008, **322**, 238.
9 A. Y. Cao, V. P. Veedu, X. S. Li, Z. L. Yao, M. N. Ghasemi-Nejhad and P. M. Ajayan, *Nat. Mater.*, 2005, **4**, 540.
10 G. Toth, J. Maklin, N. Halonen, J. Palosaari, J. Juuti, H. Jantunen, K. Kordas, W. G. Sawyer, R. Vajtai and P. M. Ajayan, *Adv. Mater.*, 2009, **21**, 2054.
11 R. Xie, C. Zhang, M. H. van der Veen, K. Arstila, T. Hantschel, B. Chen, G. Zhong and J. Robertson, *Nanotechnology*, 2013, **24**, 125603.
12 C. Subramaniam, T. Yamada, K. Kobashi, A. Sekiguchi, D. N. Futaba, M. Yumura and K. Hata, *Nat Commun*, 2013, **4**, 2202.
13 K. Hata, D. N. Futaba, K. Mizuno, T. Namai, M. Yumura and S. Iijima, *Science*, 2004, **306**, 1362.
14 R. Xiang, E. Einarsson, Y. Murakami, J. Shiomi, S. Chiashi, Z. K. Tang and S. Maruyama, *ACS Nano*, 2012, **6**, 7472.
15 G. F. Zhong, J. H. Warner, M. Fouquet, A. W. Robertson, B. A. Chen and J. Robertson, *ACS Nano*, 2012, **6**, 2893.
16 M. Hiramatsu, T. Deguchi, H. Nagao and M. Hori, *Jpn. J. Appl. Phys.*, 2007, **46**, L303.
17 K. Hasegawa and S. Noda, *ACS Nano*, 2011, **5**, 975.
18 T. Ohashi, T. Ochiai, T. Tokune and H. Kawarada, *Carbon*, 2013, **57**, 79.
19 Q. Zhang, J. Q. Huang, M. Q. Zhao, W. Z. Qian, Y. Wang and F. Wei, *Carbon*, 2008, **46**, 1152.
20 C. R. Oliver, E. S. Polsen, E. R. Meshot, S. Tawfick, S. J. Park, M. Bedewy and A. J. Hart, *ACS Nano*, 2013, **7**, 3565.
21 X. S. Li, X. F. Zhang, L. J. Ci, R. Shah, C. Wolfe, S. Kar, S. Talapatra and P. M. Ajayan, *Nanotechnology*, 2008, **19**, 455609.
22 R. G. de Villoria, A. J. Hart and B. L. Wardle, *ACS Nano*, 2011, **5**, 4850.
23 M. Xu, D. N. Futaba, T. Yamada, M. Yumura and K. Hata, *Science*, 2010, **330**, 1364.
24 J. J. Jackson, A. A. Puretzky, K. L. More, C. M. Rouleau, G. Eres and D. B. Geohegan, *ACS Nano*, 2010, **4**, 7573.
25 G. F. Zhong, T. Iwasaki, J. Robertson and H. Kawarada, *J. Phys. Chem. B*, 2007, **111**, 1907.
26 G. H. Chen, D. N. Futaba, H. Kimura, S. Sakurai, M. Yumura and K. Hata, *ACS Nano*, 2013, **7**, 10218.
27 G. H. Chen, Y. Seki, H. Kimura, S. Sakurai, M. Yumura, K. Hata and D. N. Futaba, *Sci. Rep.*, 2014, **4**, 3804.
28 S. Sakurai, M. Inaguma, D. N. Futaba, M. Yumura and K. Hat *Materials*, 2013, **6**, 2633.
29 H. Kimura, D. N. Futaba, M. Yumura and K. Hata, *J. Am. Chem Soc.*, 2012, **134**, 9219.
30 S. Esconjauregui, M. Fouquet, B. C. Bayer, C. Ducati, R. Smajda, S. Hofmann and J. Robertson, *ACS Nano*, 2010, **4**, 7431.
31 S. Sakurai, M. Inaguma, D. N. Futaba, M. Yumura and K. Hata *Small*, 2013, **9**, 3584.
32 M. Xu, D. N. Futaba, M. Yumura and K. Hata, *ACS Nano*, 2012, **6**, 5837.
33 F. Wei, Q. Zhang, W. Z. Qian, H. Yu, Y. Wang, G. H. Luo, G. H. Xu and D. Z. Wang, *Powder Technol.*, 2008, **183**, 10.
34 Available from: <http://www.zeon.co.jp/press_e/140515.html>
35 Available from: <http://www.nanocarbon.jp/sg/STD_SuperGrowthManual_EN.pdf>.
36 B. Zhao, D. N. Futaba, S. Yasuda, M. Akoshima, T. Yamada and K. Hata, *ACS Nano*, 2009, **3**, 108.
37 G. H. Chen, D. N. Futaba, S. Sakurai, M. Yumura and K. H *Carbon*, 2014, **67**, 318.
38 S. Sakurai, H. Nishino, D. N. Futaba, S. Yasuda, T. Yamada, A. Maigne, Y. Matsuo, E. Nakamura, M. Yumura and K. Hata, *J. Am. Chem. Soc.*, 2012, **134**, 2148.
39 D. N. Futaba, K. Hata, T. Namai, T. Yamada, K. Mizuno, Y. Hayamizu, M. Yumura and S. Iijima, *J. Phys. Chem. B*, 2006, **110**, 8035.
40 H. Sugime and S. Noda, *Carbon*, 2010, **48**, 2203.
41 T. Thurakitseree, E. Einarsson, R. Xiang, P. Zhao, S. Aikawa, S. Chiashi, J. Shiomi and S. Maruyama, *J. Nanosci. Nanotechnol.*, 2012, **12**, 370.
42 T. Thurakitseree, C. Kramberger, P. Zhao, S. Aikawa, S. Harish, S. Chiashi, E. Einarsson and S. Maruyama, *Carbon*, 2012, **50**, 2635.
43 H. Sugime, S. Noda, S. Maruyama and Y. Yamaguchi, *Carbon*, 2009, **47**, 234.
44 D. Y. Kim, H. Sugime, K. Hasegawa, T. Osawa and S. Noda, *Carbon*, 2012, **50**, 1538.
45 K. Hasegawa and S. Noda, *Carbon*, 2011, **49**, 4497.
46 C. Mattevi, C. T. Wirth, S. Hofmann, R. Blume, M. Cantoro, C. Ducati, C. Cepek, A. Knop-Gericke, S. Milne, C. Castellarin-Cudia, S. Dolafi, A. Goldoni, R. Schloegl and J. Robertson, *J. Phys. Chem. C*, 2008, **112**, 12207.
47 J. Kim, A. J. Page, S. Irle and K. Morokuma, *J. Am. Chem. Soc.*, 2010, **134**, 9311.
48 A. Peigney, C. Laurent, E. Flahaut, R. R. Bacsa and A. Rousset, *Carbon*, 2001, **39**, 507.
49 D. N. Futaba, J. Goto, T. Yamada, S. Yasuda, M. Yumura and K. Hata, *Carbon*, 2010, **48**, 4542.
50 S. Ata, K. Kobashi, M. Yumura and K. Hata, *Nano Lett.*, 2012, **12**, 2710.
51 T. Rueckes, K. Kim, E. Joselevich, G. Y. Tseng, C. L. Cheung and C. M. Lieber, *Science*, 2000, **289**, 94.
52 A. Izadi-Najafabadi, S. Yasuda, K. Kobashi, T. Yamada, D. N. Futaba, H. Hatori, M. Yumura, S. Iijima and K. Hata, *Adv. Mater.*, 2010, **22**, E235.
53 R. Warren, F. Sammoura, K. S. Teh, A. Kozinda, X. N. Zang and L. W. Lin, *Sens. Actuators, A: Phys.*, 2015, **231**, 65.
54 X. N. Zang, Q. Zhou, J. Y. Chang, Y. M. Liu and L. W. Lin, *Microelectron. Eng.*, 2015, **132**, 192.

55 T. de los Arcos, M. G. Garnier, P. Oelhafen, D. Mathys, J. W. Seo, C. Domingo, J. V. Garci-Ramos and S. Sanchez-Cortes, *Carbon*, 2004, **42**, 187.